CP violation in chargino decays in the MSSM

Wei Min Yang* and Dong Sheng Du
CCAST (World Laboratory), P.O. Box 8730, Beijing 100080, China
and Institute of High Energy Physics, P.O. Box 918(4), Beijing 100039, China
(Received 3 December 2002; published 11 March 2003)

In the minimal supersymmetric standard model (MSSM) with complex parameters, supersymmetric loop effects can lead to *CP* violation. We calculate the rate asymmetries of decays of charginos into the lightest neutralino and a *W* boson on the basis of the most important loop contributions in the third generation squark sector. It turns out that the *CP* violating asymmetries can be a few percent in typical regions of the parameter space of the MSSM. These processes would provide very promising channels for probing *CP* violation in the MSSM at future high-energy colliders.

DOI: 10.1103/PhysRevD.67.055004 PACS number(s): 12.60.Jv, 13.90.+i, 14.80.Ly

I. INTRODUCTION

Searching for new *CP* violating effects beyond the standard model (SM) is important and interesting work for theoretical and experimental high-energy physicists. The minimal supersymmetric standard model (MSSM) is currently considered as the most theoretically well motivated extension of the SM [1,2]. In comparison with the sole Cabibbo-Kobayashi-Maskawa (CKM) phase in the SM, it contains more diverse sources of *CP* violation through complex soft-sypersymmetry- (SUSY-)breaking parameters [3]. These new soft phases can have significant impact in a variety of places [4], including $g_\mu-2$, electric dipole moments (EDMs), *CP* violation in the *K* and *B* systems, the baryon asymmetry of the universe, cold dark matter, superpartner production cross sections and branching ratios, and rare decays. Although there are some experiments that suggest some of the phases are small, mainly the neutron and electron EDMs [5], it has recently been realized that *CP* violating phases associated with the third generation trilinear soft-breaking terms might be large and can induce sizable *CP* violation in the Higgs boson and the third generation sfermion sectors through loop corrections [6,7]. Such phases may allow baryogenesis and do not necessarily violate the stringent bound from the non-observation of EDMs [8]. In fact, some of these phases can be $\mathcal{O}(1)$, so as to provide non-SM sources of *CP* violation required for dynamical generation of the baryon asymmetry of the universe [9,10]. The important implication of the *CP* violating phases in the search for supersymmetry has received growing attention.

The decays of charginos $\tilde{\chi}_i^+$ $(i=1,2)$ and neutralinos $\tilde{\chi}_l^0$ $(l=1-4)$ in the MSSM under *CP* conservation have been extensively studied [11]. For most of the parameter space of the MSSM, the decays of the heaviest chargino $\tilde{\chi}_2^+$ and the two heavier neutralinos $\tilde{\chi}_l^0$ $(l=3,4)$ will be dominated by two-body tree-level processes in which the final states include two possible classes: (i) a lighter neutralino or chargino plus a *W*, *Z*, or Higgs boson; and (ii) channels involving squarks or sleptons if they are kinematically allowed. For the lightest chargino $\tilde{\chi}_1^+$ and the next lightest neutralino $\tilde{\chi}_2^0$, the mass difference between them and the lightest neutralino $\tilde{\chi}_1^0$ is not usually very large; therefore their dominant decay modes are three-body tree-level decays through virtual vector boson or Higgs boson mediation. But in some parameter regions, the mass splitting between them can exceed the mass of a vector boson or Higgs boson. In this case, type (i) will be their most important decay modes. Furthermore, if they are heavy enough, decay channels of type (ii) are also possible. In fact, the above decays can also occur at the one-loop level via final state interactions if they are kinematically accessible. Furthermore, the *CP* violating phases can directly affect the couplings of charginos and neutralinos to the third generation sfermions. Therefore, the interferences of the tree diagrams of these decays with the corresponding one-loop diagrams can make their partial decay widths different from those of corresponding *CP* conjugate processes. In this paper, as an example, we will focus on *CP* violation in the decays of charginos into the lightest neutralino and a *W* boson because the two-body-decay branching ratio can be large. It can be measured by the rate asymmetry:

$$A_{cp}=\frac{\Gamma(\tilde{\chi}_i^+\to\tilde{\chi}_1^0W^+)-\Gamma(\tilde{\chi}_i^-\to\tilde{\chi}_1^0W^-)}{\Gamma(\tilde{\chi}_i^+\to\tilde{\chi}_1^0W^+)+\Gamma(\tilde{\chi}_i^-\to\tilde{\chi}_1^0W^-)}. \tag{1}$$

Of course, analogous asymmetries can also be discussed for the other decay channels of charginos and neutralinos.

The remainder of this paper is organized as follows. In Sec. II we list the relevant couplings and give the analytical formulas for the decay rate asymmetries. In Sec. III, we present detailed numerical results. Our conclusions are summarized in Sec. IV. In Appendix A we outline the necessary masses and mixing matrices, and Appendix B contains the expressions for the form factors.

II. RELEVANT COUPLINGS AND DECAY RATE ASYMMETRIES

In order to calculate the rate asymmetry of decays of charginos into the lightest neutralino and a *W* boson, in Appendix A we review briefly the masses and mixing of the chargino, neutralino, and sfermion sectors of the MSSM. As

*Email address: yangwm@mail.ihep.ac.cn

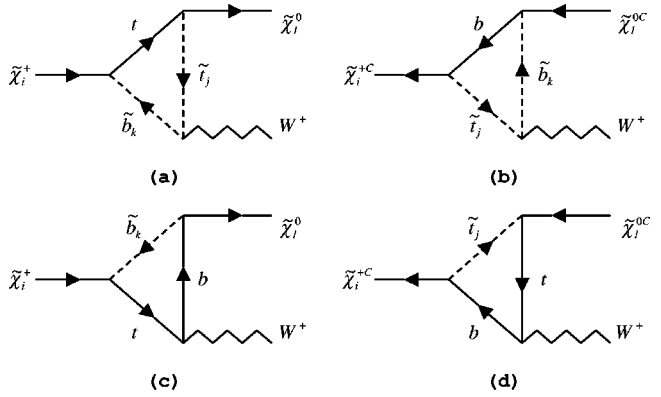

FIG. 1. The relevant one-loop diagrams for the decay $\tilde{\chi}_i^+ \to \tilde{\chi}_1^0 W^+$.

mentioned in the last section, although the tree-level decay of charginos is invariant under CP, a nonvanishing value of the rate asymmetry A_{cp} in Eq. (1) is generated at the one-loop level by complex couplings. Among others, the most significant CP violating effects arise from the trilinear couplings of the third generation $A_{t,b,\tau}$ [12], especially from the squark sectors because of the the Yukawa characteristic factor m_q (m_q is the mass of the quark q) in the chargino- or neutralino-quark-squark couplings. Therefore, one can expect that the most important contributions come from one-loop quark-squark exchange diagrams, as shown in Figs. 1(a)–1(d). The relevant interaction Lagrangians are as follows [1]:

$$\mathcal{L}_{\tilde{\chi}^+ q\tilde{q}'} = \overline{t}(A_{ik}^L P_L + A_{ik}^R P_R)\tilde{\chi}_i^+ \tilde{b}_k + \overline{b}(B_{ij}^L P_L + B_{ij}^R P_R)\tilde{\chi}_i^{+c}\tilde{t}_j + \overline{\tilde{\chi}_i^+}(A_{ik}^{R*} P_L + A_{ik}^{L*} P_R) t\tilde{b}_k^* + \overline{\tilde{\chi}_i^{+c}}(B_{ij}^{R*} P_L + B_{ij}^{L*} P_R) b\tilde{t}_j^*,$$

$$\mathcal{L}_{\tilde{\chi}^0 q\tilde{q}} = \overline{t}(C_{lj}^L P_L + C_{lj}^R P_R)\tilde{\chi}_l^0 \tilde{t}_j + \overline{b}(D_{lk}^L P_L + D_{lk}^R P_R)\tilde{\chi}_l^0 \tilde{b}_k + \overline{\tilde{\chi}_l^0}(C_{lj}^{R*} P_L + C_{lj}^{L*} P_R) t\tilde{t}_j^* + \overline{\tilde{\chi}_l^0}(D_{lk}^{R*} P_L + D_{lk}^{L*} P_R) b\tilde{b}_k^*,$$

$$\mathcal{L}_{W\tilde{\chi}^0\tilde{\chi}^+} = W_\mu^- \overline{\tilde{\chi}_l^0}\gamma^\mu(E_{il}^L P_L + E_{il}^R P_R)\tilde{\chi}_i^+ + W_\mu^+ \overline{\tilde{\chi}_i^+}\gamma^\mu(E_{il}^{L*} P_L + E_{il}^{R*} P_R)\tilde{\chi}_l^0,$$

$$\mathcal{L}_{W\tilde{q}\tilde{q}'} = i(F_{kj} W_\mu^- \tilde{b}_k^* \overleftrightarrow{\partial}_\mu \tilde{t}_j + F_{kj}^* W_\mu^+ \tilde{t}_j^* \overleftrightarrow{\partial}_\mu \tilde{b}_k),$$

$$\mathcal{L}_{Wqq'} = -\frac{g}{\sqrt{2}}(W_\mu^- \overline{b}\gamma^\mu P_L t + W_\mu^+ \overline{t}\gamma^\mu P_L b), \tag{2}$$

where $j,k=(1,2)$, and $P_{L,R}=(1\mp\gamma^5)/2$. The corresponding coupling coefficients are given by

$$A_{ik}^L = \frac{g m_t}{\sqrt{2} m_W s_\beta} V_{i2}^* R_{k1}^{\tilde{b}*},$$

$$A_{ik}^R = \frac{g}{\sqrt{2}}\left[\frac{m_b}{m_W c_\beta} U_{i2} R_{k2}^{\tilde{b}*} - \sqrt{2} U_{i1} R_{k1}^{\tilde{b}*}\right],$$

$$B_{ij}^L = \frac{g m_b}{\sqrt{2} m_W c_\beta} U_{i2}^* R_{j1}^{\tilde{t}*},$$

$$B_{ij}^R = \frac{g}{\sqrt{2}}\left[\frac{m_t}{m_W s_\beta} V_{i2} R_{j2}^{\tilde{t}*} - \sqrt{2} V_{i1} R_{j1}^{\tilde{t}*}\right],$$

$$C_{lj}^L = \frac{g}{\sqrt{2}}\left[-\frac{m_t}{m_W s_\beta} N_{l4}^* R_{j1}^{\tilde{t}*} + \frac{4}{3}\tan\theta_W N_{l1}^* R_{j2}^{\tilde{t}*}\right],$$

$$C_{lj}^R = \frac{g}{\sqrt{2}}\left[-\frac{m_t}{m_W s_\beta} N_{l4} R_{j2}^{\tilde{t}*} - \left(N_{l2} + \frac{1}{3}\tan\theta_W N_{l1}\right) R_{j1}^{\tilde{t}*}\right],$$

$$D_{lk}^L = \frac{g}{\sqrt{2}}\left[-\frac{m_b}{m_W c_\beta} N_{l3}^* R_{k1}^{\tilde{b}*} - \frac{2}{3}\tan\theta_W N_{l1}^* R_{k2}^{\tilde{b}*}\right],$$

$$D_{lk}^R = \frac{g}{\sqrt{2}}\left[-\frac{m_b}{m_W c_\beta} N_{l3} R_{k2}^{\tilde{b}*} + \left(N_{l2} - \frac{1}{3}\tan\theta_W N_{l1}\right) R_{k1}^{\tilde{b}*}\right],$$

$$E_{il}^L = \frac{g}{\sqrt{2}}(\sqrt{2} V_{i1}^* N_{l2} - V_{i2}^* N_{l4}),$$

$$E_{il}^R = \frac{g}{\sqrt{2}}(\sqrt{2} U_{i1} N_{l2}^* + U_{i2} N_{l3}^*),$$

$$F_{kj} = -\frac{g}{\sqrt{2}} R_{k1}^{\tilde{b}} R_{j1}^{\tilde{t}*}. \tag{3}$$

The total amplitude of the $\tilde{\chi}_i^\pm \to \tilde{\chi}_1^0 W^\pm$ processes can be written as

$$\mathcal{M}(\tilde{\chi}_i^\pm \to \tilde{\chi}_1^0 W^\pm) = \mathcal{M}_{tree}^{(\pm)} + \mathcal{M}_{loop}^{(\pm)} \tag{4}$$

with

$$\mathcal{M}_{tree}^{(+)} = \overline{u}_{\tilde{\chi}_1^0}(k_1)\gamma^\mu(E_{i1}^L P_L + E_{i1}^R P_R) u_{\tilde{\chi}_i^+}(p)\epsilon_\mu(k_2), \tag{5}$$

$$\mathcal{M}_{tree}^{(-)} = \overline{v}_{\tilde{\chi}_i^+}(-p)\gamma^\mu(E_{i1}^{L*} P_L + E_{i1}^{R*} P_R) \times v_{\tilde{\chi}_1^0}(-k_1)\epsilon_\mu^*(-k_2),$$

$$\mathcal{M}_{loop}^{(+)} = \overline{u}_{\tilde{\chi}_1^0}(k_1)[(\gamma^\mu \Lambda_{(+)i1}^L + p^\mu \Pi_{(+)i1}^L) P_L + (\gamma^\mu \Lambda_{(+)i1}^R + p^\mu \Pi_{(+)i1}^R) P_R] u_{\tilde{\chi}_i^+}(p)\epsilon_\mu(k_2),$$

$$\mathcal{M}^{(-)}_{loop} = \overline{v}_{\tilde{\chi}_i^+}(-p)[(\gamma^\mu \Lambda^L_{(-)i1} + p^\mu \Pi^R_{(-)i1})P_L + (\gamma^\mu \Lambda^R_{(-)i1} + p^\mu \Pi^L_{(-)i1})P_R] \times v_{\tilde{\chi}_1^0}(-k_1)\epsilon^*_\mu(-k_2),$$

where $\Lambda^{L,R}_{(\pm)}$ and $\Pi^{L,R}_{(\pm)}$ represent the form factors of vertex corrections contributed by the one-loop diagrams in Fig. 1, whose expressions are listed in Appendix B. At next-to-leading order, the *CP* violating asymmetry of Eq. (1) can be obtained as

$$A_{cp} = \frac{2\rho \mathrm{Re}\delta G - 12 m_{\tilde{\chi}_i^+} m_{\tilde{\chi}_1^0} m_W^2 \mathrm{Re}\delta H + \lambda(m_{\tilde{\chi}_1^0}\mathrm{Re}\delta I + m_{\tilde{\chi}_i^+}\mathrm{Re}\delta J)}{2\rho(|E^L_{i1}|^2 + |E^R_{i1}|^2) - 24 m_{\tilde{\chi}_i^+} m_{\tilde{\chi}_1^0} m_W^2 \mathrm{Re}(E^L_{i1} E^{R*}_{i1})} \tag{6}$$

with

$$\rho = m_W^2(m^2_{\tilde{\chi}_i^+} + m^2_{\tilde{\chi}_1^0} - 2m_W^2) + (m^2_{\tilde{\chi}_i^+} - m^2_{\tilde{\chi}_1^0})^2,$$

$$\lambda = m^2_{\tilde{\chi}_i^+} + m^2_{\tilde{\chi}_1^0} + m_W^2 - 2m_{\tilde{\chi}_i^+} m_{\tilde{\chi}_1^0} - 2m_{\tilde{\chi}_i^+} m_W - 2m_{\tilde{\chi}_1^0} m_W, \tag{7}$$

and

$$\delta G = (\Lambda^L_{(+)i1} E^{L*}_{i1} + \Lambda^R_{(+)i1} E^{R*}_{i1}) - (\Lambda^L_{(-)i1} E^L_{i1} + \Lambda^R_{(-)i1} E^R_{i1}),$$

$$\delta H = (\Lambda^L_{(+)i1} E^{R*}_{i1} + \Lambda^R_{(+)i1} E^{L*}_{i1}) - (\Lambda^L_{(-)i1} E^R_{i1} + \Lambda^R_{(-)i1} E^L_{i1}),$$

$$\delta I = (\Pi^L_{(+)i1} E^{L*}_{i1} + \Pi^R_{(+)i1} E^{R*}_{i1}) - (\Pi^L_{(-)i1} E^L_{i1} + \Pi^R_{(-)i1} E^R_{i1}),$$

$$\delta J = (\Pi^L_{(+)i1} E^{R*}_{i1} + \Pi^R_{(+)i1} E^{L*}_{i1}) - (\Pi^L_{(-)i1} E^R_{i1} + \Pi^R_{(-)i1} E^L_{i1}). \tag{8}$$

From Eqs. (6)–(8), it can be seen directly that there is no *CP* violation at the tree level because of all the form factors vanishing. However, in order to generate *CP* violation effects, loop corrections (viz., nonvanishing form factors) and complex couplings (viz., nonvanishing *CP* violating phases) are essential factors.

III. NUMERICAL RESULTS

In this section, we will illustrate the numerical results for *CP* violating asymmetry based on the MSSM parameter space at the electroweak scale allowed by the present data constraints [13]. In order not to vary too many parameters, we assume the grand unified theory relation for the gaugino mass parameters, $M_1 \approx 0.5 M_2$. In this case, the phase of the gaugino sector can be rotated away. In addition, since the phase of the Higgs mixing parameter φ_μ is highly constrained by the EDMs of the electron and neutron [5], we take $\varphi_\mu = 0$. For the mass parameters of the squark sectors, we simply fix the relations $M_{\tilde{U}} : M_{\tilde{Q}} : M_{\tilde{D}} \approx 0.85 : 1 : 1.05$. Thus, in our following numerical analyses the input parameters contain only $M_2, M_{\tilde{Q}}, |\mu|, |A_t|, |A_b|, \varphi_t, \varphi_b$, and $\tan\beta$. For the set of representative values in the parameter space

$$M_2 = 250 \text{ GeV}, \quad M_{\tilde{Q}} = 450 \text{ GeV}, \quad |\mu| = 500 \text{ GeV},$$

$$|A_t| = |A_b| = 500 \text{ GeV}, \quad \varphi_t = \varphi_b = \frac{\pi}{4}, \quad \tan\beta = 5 \text{ or } 40, \tag{9}$$

we list the relevant sparticle masses explicitly in Table I. It can be seen that because of the large Yukawa couplings of the third generation squarks, the mixing between top or bottom squarks can be very strong, especially for the high value of $\tan\beta = 40$. Moreover, the masses of $\tilde{\chi}_1^0$ and $\tilde{\chi}_1^+$ approximate to the values of M_1 and M_2, respectively, while the mass of $\tilde{\chi}_2^+$ is about the value of $|\mu|$. In fact, this is generic in the region $|\mu| \geq M_2$ [11]. Therefore, if M_2 and $|\mu|$ are not too low, both $\tilde{\chi}_1^\pm \to \tilde{\chi}_1^0 W^\pm$ and $\tilde{\chi}_2^\pm \to \tilde{\chi}_1^0 W^\pm$ are kinematically allowed.

We now consider only the $\tilde{\chi}_2^\pm \to \tilde{\chi}_1^0 W^\pm$ channel, and demonstrate in turn the dependence of its *CP* violating asymmetry A_{cp} on various choices of the parameters. Because our results are not sensitive to M_2, it will be fixed. In Fig. 2, the absolute value of the *CP* asymmetry, $|A_{cp}|$, is shown as a function of the Higgs mixing parameter $|\mu|$. The four curves in this figure correspond to the four combined choices of $\tan\beta = 5$ (or 40) and $\varphi_t = \varphi_b = \pi/4$ (or $\pi/2$), respectively. The other parameters are fixed by Eq. (9). From these curves, for instance, for the short-dashed line of $\tan\beta = 5$ and $\varphi_t = \varphi_b = \pi/4$, one can distinguish the thresholds of $b\tilde{t}_1$ at $|\mu| \approx 295$ GeV, $b\tilde{t}_2$ at $|\mu| \approx 495$ GeV, $t\tilde{b}_1$ at $|\mu| \approx 610$ GeV, and $t\tilde{b}_2$ at $|\mu| \approx 650$ GeV. In the region of small $|\mu|$, the contributions to $|A_{cp}|$ come from the top-squark–bottom-quark–bottom-squark loop of Fig. 2(b) and the top–squark–bottom–top-quark loop of Fig. 2(d). As can be seen, once $m_{\tilde{\chi}_2^+} > m_b + m_{\tilde{t}_1}$, $|A_{cp}|$ can sharply go up to the

TABLE I. The relevant sparticle masses (in GeV) for the parameter sets in Eq. (9).

$\tan\beta$	$m_{\tilde{\chi}_1^+}$	$m_{\tilde{\chi}_2^+}$	$m_{\tilde{\chi}_1^0}$	$m_{\tilde{t}_1}$	$m_{\tilde{t}_2}$	$m_{\tilde{b}_1}$	$m_{\tilde{b}_2}$
5	236	519	122	350	532	449	477
40	241	517	124	336	541	361	548

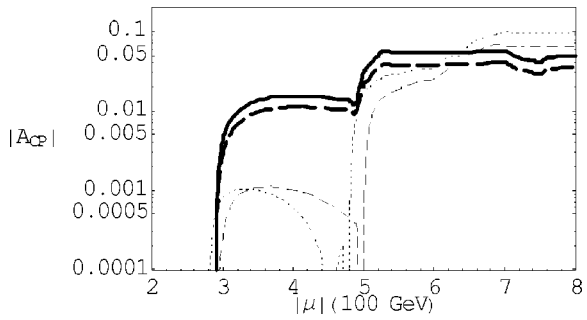

FIG. 2. Absolute value of A_{cp} as a function of $|\mu|$ for $M_2=250$ GeV, $M_{\tilde{Q}}=450$ GeV, and $|A_t|=|A_b|=500$ GeV. The thinner short-dashed line (dotted line) is for $\tan\beta=5,\varphi_t=\varphi_b=\pi/4(\pi/2)$, and the thicker long-dashed line (solid line) is for $\tan\beta=40,\varphi_t=\varphi_b=\pi/4\ (\pi/2)$.

order of 10^{-3} (10^{-2}) for $\tan\beta=5$ $(\tan\beta=40)$. As the value of $|\mu|$ increases, with the $\tilde{\chi}_2^+\to b\tilde{t}_2$ channel open, $|A_{cp}|$ can further rise to several percent whether $\tan\beta=5$ or 40. For larger $|\mu|$, one should however take the contributions of diagram (a) and (c) in Fig. 2 into account though they are relatively smaller.

In Fig. 3, we plot $|A_{cp}|$ as a function of the left-handed soft-SUSY-breaking squark mass $M_{\tilde{Q}}$ for the same arrangement of $\tan\beta$ and φ_t,φ_b as in Fig. 2. The other parameters are still given by Eq. (9). Here it is more clearly visible that the threshold of $b\tilde{t}_2$ is at $M_{\tilde{Q}}\approx 455$ (470) GeV for $\tan\beta=5$ and $\varphi_t=\varphi_b=\pi/4\ (\pi/2)$, and at $M_{\tilde{Q}}\approx 460$ (465) GeV for $\tan\beta=40$ and $\varphi_t=\varphi_b=\pi/4\ (\pi/2)$. For $\tan\beta=40$, $|A_{cp}|$ is essentially of the order of 10^{-2} in the region $M_{\tilde{Q}}=300-600$ GeV. For $\tan\beta=5$, in the lighter squark region, namely, above the threshold of $\tilde{\chi}_2^+\to b\tilde{t}_2$, $|A_{cp}|$ is also of the order of 10^{-2}; in the heavier squark region, the $\tilde{\chi}_2^+\to b\tilde{t}_2$ channel is closed, and $|A_{cp}|$ is reduced to the order of 10^{-3}.

The CP asymmetry as a function of the trilinear coupling $|A_t|=|A_b|$ is illustrated in Fig. 4. Here we take $|\mu|=550$ GeV, the other parameters are still fixed by Eq. (9), and the choices of $\tan\beta,\varphi_t,\varphi_b$ are the same as the previous values. For smaller values of $|A_t|=|A_b|$, $|A_{cp}|$ is very small and below $\mathcal{O}(0.01)$. As $|A_t|=|A_b|$ increases from small to large, $|A_{cp}|$ rises to a few percent. On the other hand, on changing $\tan\beta=5$ to $\tan\beta=40$, the values of $|A_{cp}|$ are raised 2% or so; varying $\varphi_t=\varphi_b$ from $\pi/4$ to $\pi/2$, $|A_{cp}|$ is enhanced by about 0.01.

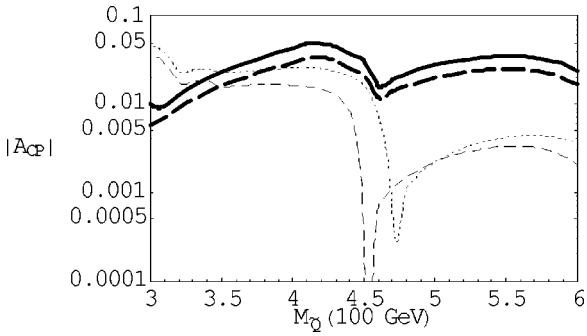

FIG. 3. $|A_{cp}|$ as a function of $M_{\tilde{Q}}$ for $|\mu|=500$ GeV, $M_2=250$ GeV, and $|A_t|=|A_b|=500$ GeV. The thinner short-dashed line (dotted line) is for $\tan\beta=5,\varphi_t=\varphi_b=\pi/4(\pi/2)$, and the thicker long-dashed line (solid line) is for $\tan\beta=40,\varphi_t=\varphi_b=\pi/4(\pi/2)$.

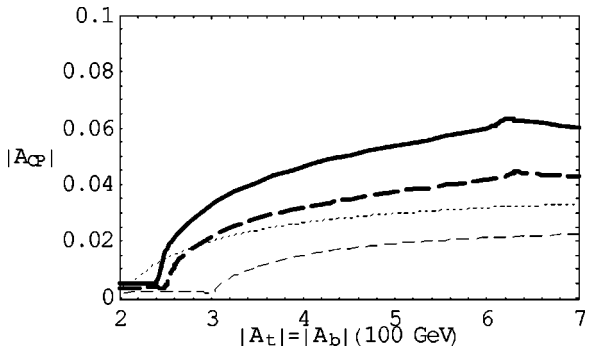

FIG. 4. $|A_{cp}|$ as a function of $|A_t|=|A_b|$ for $|\mu|=550$ GeV, $M_{\tilde{Q}}=450$ GeV, and $M_2=250$ GeV. The thinner short-dashed line (dotted line) is for $\tan\beta=5,\varphi_t=\varphi_b=\pi/4(\pi/2)$, and the thicker long-dashed line (solid line) is for $\tan\beta=40,\varphi_t=\varphi_b=\pi/4(\pi/2)$.

Figure 5 shows the dependence of A_{cp} on the CP violating phase φ_t for the four combined choices of $\tan\beta=5$ and 40 and $\varphi_b=0$ and φ_t. Here we take $|\mu|=600$ GeV and $M_{\tilde{Q}}=400$ GeV; the other parameters are given by Eq. (9). As expected, A_{cp} shows $\sim\sin\varphi_t$ dependence. For the case of $\tan\beta=5$, because the value of $|\mu|$ is larger than the value of $M_{\tilde{Q}}$, all of the $b\tilde{t}_{1,2}$, $t\tilde{b}_{1,2}$ channels are open. At the two maximal top squark phases $\varphi_t=\pi/2,3\pi/2$, the CP asymmetry can reach 6%. In this case, because the mixing between bottom squarks is not very large, the influence of the phase φ_b is relatively small. For the case of $\tan\beta=40$, however, the mixing between bottom squarks is comparable with the mixing between top squarks, and φ_b can obviously change A_{cp} by up to 40% at $\varphi_t=\pi/2,3\pi/2$.

IV. CONCLUSIONS

In this work, we have discussed possible CP violation in the decays of charginos and neutralinos in the MSSM. For the decay of the heaviest chargino into the lightest neutralino

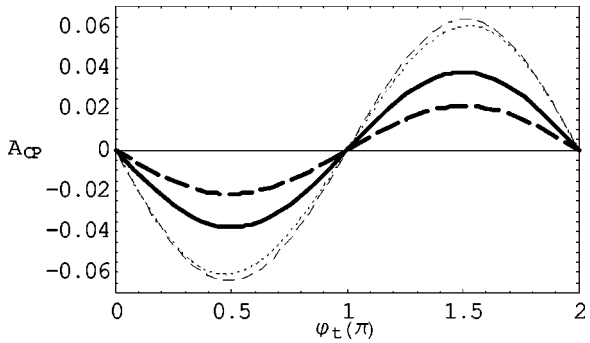

FIG. 5. A_{cp} as a function of φ_t for $M_{\tilde{Q}}=400$ GeV, $|\mu|=600$ GeV, $M_2=250$ GeV, and $|A_t|=|A_b|=500$ GeV. The thinner short-dashed line (dotted line) is for $\tan\beta=5,\varphi_b=0(\varphi_t)$, and the thicker long-dashed line (solid line) is for $\tan\beta=40,\varphi_b=0\ (\varphi_t)$.

and a W boson, we have explicitly presented analytical and numerical results for the CP violating asymmetry. The decay rate asymmetry originates from the large CP violating phases and one-loop corrections of the third generation squark sectors. The CP asymmetry can typically reach several percent, depending mainly on the phases and $\tan\beta$. For a larger mixing between the top squarks (bottom squarks), the CP asymmetry is particularly evident. At a future e^+e^- linear collider with $\sqrt{s}=500$–1000 GeV [14], the cross section of chargino pair production is around $\mathcal{O}(1)$ pb [15]. With a integrated luminosity $\mathcal{L}=100$ fb^{-1}, about several hundred signal events can be expected since the decay channels have a larger branching ratio and a cleaner final signal. Therefore, analyzing these final states would allow us to measure the important couplings of squark sectors and determine the CP violating phases, thus providing an opportunity for detecting directly the CP violating effects of the MSSM.

ACKNOWLEDGMENTS

One of the authors, W.M.Y., thanks M. Z. Yang for helpful discussions. This work is in part supported by the National Natural Science Foundation of China.

APPENDIX A: SUSY PARTICLES MASSES AND MIXING

To fix our notation, we simply summarize in this appendix the masses and mixing of the relevant sparticles. The mass matrices of charginos and neutralinos are given, respectively, by

$$M_C=\begin{pmatrix} M_2 & \sqrt{2}m_W s_\beta \\ \sqrt{2}m_W c_\beta & \mu \end{pmatrix} \tag{A1}$$

and

$$M_N=\begin{pmatrix} M_1 & 0 & -m_Z s_W c_\beta & m_Z s_W s_\beta \\ 0 & M_2 & m_Z c_W c_\beta & -m_Z c_W s_\beta \\ -m_Z s_W c_\beta & m_Z c_W c_\beta & 0 & -\mu \\ m_Z s_W s_\beta & -m_Z c_W s_\beta & -\mu & 0 \end{pmatrix}, \tag{A2}$$

where we have used the abbreviations $s_W=\sin\theta_W$, $c_\beta=\cos\beta$, etc. M_1 and M_2 are the soft-SUSY-breaking gaugino mass parameters. μ is the Higgs mixing parameter. $\tan\beta$ is the ratio of the two Higgs vacuum expectation values. μ and one of $M_i (i=1,2)$ can be complex. The chargino mass matrix can be diagonalized by two unitary matrices U and V,

$$U^* M_C V^\dagger = \mathrm{diag}(m_{\tilde{\chi}_1^+}, m_{\tilde{\chi}_2^+}), \tag{A3}$$

where $m_{\tilde{\chi}_{1,2}^+}$ are the masses of the physical chargino states. The neutralino mass matrix can be diagonalized by a single unitary matrix N,

$$N^* M_N N^\dagger = \mathrm{diag}(m_{\tilde{\chi}_1^0}, m_{\tilde{\chi}_2^0}, m_{\tilde{\chi}_3^0}, m_{\tilde{\chi}_4^0}), \tag{A4}$$

where $m_{\tilde{\chi}_l^0} (l=1$–$4)$ are the masses of the physical neutralino states. The expressions for the mass eigenvalues and mixing matrix elements for charginos and neutralinos can be found in Ref. [11].

The mass-squared matrices of top and bottom squarks in the left-right basis can be written as

$$M_{\tilde{q}}^2=\begin{pmatrix} m_{LL}^2 & m_{LR}^2 \\ m_{LR}^{2*} & m_{RR}^2 \end{pmatrix} \quad (q=t/b) \tag{A5}$$

with

$$\begin{aligned} m_{LL}^2 &= M_{\tilde{Q}}^2 + m_q^2 + m_Z^2 \cos 2\beta (T_3^q - Q_q s_W^2), \\ m_{RR}^2 &= M_{\tilde{U}/\tilde{D}}^2 + m_q^2 + m_Z^2 \cos 2\beta Q_q s_W^2, \\ m_{LR}^2 &= m_q (A_q^* - \mu \cot\beta)/m_q (A_q^* - \mu \tan\beta), \end{aligned} \tag{A6}$$

where $M_{\tilde{Q}}$ and $M_{\tilde{U}}$ ($M_{\tilde{D}}$) are the left- and right-handed soft-SUSY-breaking top squark (bottom squark) masses, respectively. The soft-SUSY-breaking trilinear couplings A_q are complex parameters,

$$A_t = |A_t| e^{i\varphi_t}, \quad A_b = |A_b| e^{i\varphi_b} \tag{A7}$$

with CP violating phases φ_t and φ_b. The mass-squared matrix $M_{\tilde{q}}^2$ can be diagonalized by a unitary matrix $R^{\tilde{q}}$,

$$R^{\tilde{q}} M_{\tilde{q}}^2 R^{\tilde{q}\,\dagger} = \mathrm{diag}(m_{\tilde{q}_1}^2, m_{\tilde{q}_2}^2), \tag{A8}$$

where the diagonalization matrix can be parametrized as

$$R^{\tilde{q}}=\begin{pmatrix} \cos\theta_q & \sin\theta_q e^{i\delta_q} \\ -\sin\theta_q e^{-i\delta_q} & \cos\theta_q \end{pmatrix} \tag{A9}$$

with

$$\delta_t = \arg(A_t^* - \mu\cot\beta), \quad \delta_b = \arg(A_b^* - \mu\tan\beta). \tag{A10}$$

The squark mass eigenvalues and mixing angle are then given by

$$\begin{aligned} m_{\tilde{q}_{1,2}}^2 &= \frac{1}{2}[m_{LL}^2 + m_{RR}^2 \mp \sqrt{(m_{LL}^2 - m_{RR}^2)^2 + 4|m_{LR}^2|^2}], \\ \tan\theta_q &= \frac{2|m_{LR}^2|}{m_{LL}^2 - m_{RR}^2 + m_{\tilde{q}_1}^2 - m_{\tilde{q}_2}^2}. \end{aligned} \tag{A11}$$

APPENDIX B: THE RELEVANT FORM FACTORS

In this appendix, we list the form factors of the one-loop corrections in Fig. 1. We give only the form factors of the decay $\tilde{\chi}_i^+ \to \tilde{\chi}_l^0 W^+$, $\Lambda_{(+)il}^{L,R}$ and $\Pi_{(+)il}^{L,R}$. Those of the decay $\tilde{\chi}_i^- \to \tilde{\chi}_l^0 W^-$, $\Lambda_{(-)il}^{L,R}$ and $\Pi_{(-)il}^{L,R}$ can be obtained correspondingly by conjugating all the couplings in $\Lambda_{(+)il}^{L,R}$ and $\Pi_{(+)il}^{L,R}$. Corresponding to the four one-loop diagram contributions, the form factors $\Lambda_{(+)il}^{L,R}$ and $\Pi_{(+)il}^{L,R}$ [in the following we omit

"(+)"] can be divided into four parts,

$$\Lambda_{il}^{L,R}=\Lambda_{il}^{(1)L,R}+\Lambda_{il}^{(2)L,R}+\Lambda_{il}^{(3)L,R}+\Lambda_{il}^{(4)L,R},$$
$$\Pi_{il}^{L,R}=\Pi_{il}^{(1)L,R}+\Pi_{il}^{(2)L,R}+\Pi_{il}^{(3)L,R}+\Pi_{il}^{(4)L,R} \tag{B1}$$

with

$$\Lambda_{il}^{(1)L}=\frac{3}{8\pi^2}\sum_{j,k} A_{ik}^{L}C_{lj}^{L*}F_{kj}C_{24}^{(1)}, \quad \Lambda_{il}^{(1)R}=\Lambda_{il}^{(1)L}(L\leftrightarrow R),$$

$$\Lambda_{il}^{(2)L}=\frac{3}{8\pi^2}\sum_{j,k} B_{ij}^{L*}D_{lk}^{L}F_{kj}C_{24}^{(2)}, \quad \Lambda_{il}^{(2)R}=\Lambda_{il}^{(2)L}(L\leftrightarrow R),$$

$$\Lambda_{il}^{(3)L}=\frac{3g}{16\sqrt{2}\pi^2}\sum_{k}\Big\{m_b m_{\tilde{\chi}_l^0}A_{ik}^{L}D_{lk}^{R*}C_{12}^{(3)} - m_t m_{\tilde{\chi}_i^+}A_{ik}^{R}D_{lk}^{L*}(C_0^{(3)}+C_{11}^{(3)})+A_{ik}^{L}D_{lk}^{L*}\Big[\frac{1}{2}+2C_{24}^{(3)} + m_{\tilde{\chi}_i^+}^2(C_{11}^{(3)}-C_{12}^{(3)}+C_{21}^{(3)}-C_{23}^{(3)})+m_{\tilde{\chi}_l^0}^2 \times(C_{22}^{(3)}-C_{23}^{(3)})+m_W^2(C_{12}^{(3)}+C_{23}^{(3)})\Big]\Big\},$$

$$\Lambda_{il}^{(3)R}=\frac{3g}{16\sqrt{2}\pi^2}\sum_{k}\{-m_t m_b A_{ik}^{R}D_{lk}^{R*}C_0^{(3)} + m_b m_{\tilde{\chi}_i^+}A_{ik}^{L}D_{lk}^{R*}C_{11}^{(3)}-m_t m_{\tilde{\chi}_l^0}A_{ik}^{R}D_{lk}^{L*}(C_0^{(3)}+C_{12}^{(3)}) + m_{\tilde{\chi}_i^+}m_{\tilde{\chi}_l^0}A_{ik}^{L}D_{lk}^{L*}(C_{11}^{(3)}-C_{12}^{(3)})\},$$

$$\Lambda_{il}^{(4)L,R}=\Lambda_{il}^{(3)L,R}(A_{ik}^{L,R}\leftrightarrow C_{lk}^{L,R}, D_{lk}^{L,R}\leftrightarrow B_{ik}^{L,R}, m_{\tilde{\chi}_i^+}\leftrightarrow m_{\tilde{\chi}_l^0}, C_{0,11,12,21,22,23,24}^{(3)}\leftrightarrow C_{0,11,12,21,22,23,24}^{(4)}),$$

$$\Pi_{il}^{(1)L}=-\frac{3}{16\pi^2}\sum_{j,k} F_{kj}[m_t A_{ik}^{L}C_{lj}^{R*}(C_{11}^{(1)}-C_{12}^{(1)}) + m_{\tilde{\chi}_l^0}A_{ik}^{L}C_{lj}^{L*}(C_{22}^{(1)}-C_{23}^{(1)})+m_{\tilde{\chi}_i^+}A_{ik}^{R}C_{lj}^{R*} \times(C_{11}^{(1)}-C_{12}^{(1)}+C_{21}^{(1)}-C_{23}^{(1)})],$$

$$\Pi_{il}^{(1)R}=\Pi_{il}^{(1)L}(L\leftrightarrow R),$$

$$\Pi_{il}^{(2)L}=-\frac{3}{16\pi^2}\sum_{j,k} F_{kj}[m_b B_{ij}^{R*}D_{lk}^{L}(C_{11}^{(2)}-C_{12}^{(2)}) + m_{\tilde{\chi}_i^+}B_{ij}^{L*}D_{lk}^{L}(C_{22}^{(2)}-C_{23}^{(2)})+m_{\tilde{\chi}_l^0}B_{ij}^{R*}D_{lk}^{R} \times(C_{11}^{(2)}-C_{12}^{(2)}+C_{21}^{(2)}-C_{23}^{(2)})],$$

$$\Pi_{il}^{(2)R}=\Pi_{il}^{(2)L}(L\leftrightarrow R),$$

$$\Pi_{il}^{(3)L}=\frac{3g}{16\sqrt{2}\pi^2}\sum_{k}[m_b A_{ik}^{L}D_{lk}^{R*}C_{12}^{(3)}+m_{\tilde{\chi}_l^0}A_{ik}^{L}D_{lk}^{L*} \times(C_{22}^{(3)}-C_{23}^{(3)})],$$

$$\Pi_{il}^{(3)R}=\frac{3g}{16\sqrt{2}\pi^2}\sum_{k}[-m_t A_{ik}^{R}D_{lk}^{L*}(C_0^{(3)}+C_{11}^{(3)}) + m_{\tilde{\chi}_i^+}A_{ik}^{L}D_{lk}^{L*}(C_{11}^{(3)}-C_{12}^{(3)}+C_{21}^{(3)}-C_{23}^{(3)})],$$

$$\Pi_{il}^{(4)L,R}=\Pi_{il}^{(3)L,R}(A_{ik}^{L,R}\leftrightarrow C_{lk}^{L,R}, D_{lk}^{L,R}\leftrightarrow B_{ik}^{L,R}, m_{\tilde{\chi}_i^+}\leftrightarrow m_{\tilde{\chi}_l^0}, C_{0,11,12,21,22,23}^{(3)}\leftrightarrow C_{0,11,12,21,22,23}^{(4)}), \tag{B2}$$

where

$$C_{11,12,21,22,23,24}^{(1)}=C_{11,12,21,22,23,24}\times(m_{\tilde{\chi}_l^0}^2, m_{\tilde{\chi}_i^+}^2, m_W^2, m_{\tilde{t}_j}^2, m_t^2, m_{\tilde{b}_k}^2),$$

$$C_{11,12,21,22,23,24}^{(2)}=C_{11,12,21,22,23,24}\times(m_{\tilde{\chi}_l^0}^2, m_{\tilde{\chi}_i^+}^2, m_W^2, m_{\tilde{b}_k}^2, m_b^2, m_{\tilde{t}_j}^2),$$

$$C_{0,11,12,21,22,23,24}^{(3)}=C_{0,11,12,21,22,23,24}\times(m_{\tilde{\chi}_l^0}^2, m_{\tilde{\chi}_i^+}^2, m_W^2, m_b^2, m_{\tilde{b}_k}^2, m_t^2),$$

$$C_{0,11,12,21,22,23,24}^{(4)}=C_{0,11,12,21,22,23,24}\times(m_{\tilde{\chi}_l^0}^2, m_{\tilde{\chi}_i^+}^2, m_W^2, m_t^2, m_{\tilde{t}_j}^2, m_b^2). \tag{B3}$$

The definitions and numerical calculation formulas of the Passarino-Veltman one-, two-, and three-point functions are adopted from Ref. [16].

[1] H.P. Nilles, Phys. Rep. **110**, 1 (1984); H. Haber and G. Kane, *ibid.* **117**, 75 (1985).

[2] M. Drees, hep-ph/9611409; S.P. Martin, hep-ph/9709356; M. Peskin, hep-ph/9705479; D.I. Kazakov, hep-ph/0012288.

[3] S. Dimopoulos and D. Sutter, Nucl. Phys. **B452**, 496 (1996).

[4] A. Masiero and O. Vives, Nucl. Phys. B (Proc. Suppl.) **101**, 253 (2001); T. Ibrahim and P. Nath, hep-ph/0107325.

[5] I.S. Altarev *et al.*, Phys. Lett. B **276**, 242 (1992); Y. Kizukuri and N. Oshimo, Phys. Rev. D **46**, 3025 (1992); R. Garisto and J.D. Wells, *ibid.* **55**, 1611 (1997).

[6] A. Pilaftsis, Phys. Lett. B **435**, 88 (1998); D.A. Demir, Phys. Rev. D **60**, 055006 (1999); M. Carena, J. Ellis, A. Pilaftsis, and C.E.M. Wagner, Nucl. Phys. **B586**, 92 (2000).

[7] E. Christova, H. Eberl, S. Kraml, and W. Majerotto, Nucl. Phys. **B639**, 263 (2002); W.M. Yang and D.S. Du, Phys. Rev. D **65**, 115005 (2002).

[8] M. Carena, J.M. Moreno, M. Quiros, M. Seco, and C.E. Wagner, Nucl. Phys. **B599**, 158 (2001); T. Ibrahim and P. Nath, Phys. Lett. B **418**, 98 (1998); M. Brhlik, G.J. Good, and G.L. Kane, Phys. Rev. D **63**, 035002 (2001).

[9] T. Falk and K.V. Olive, Phys. Lett. B **439**, 71 (1998); M. Carena, M. Quiros, and C.E. Wagner, Nucl. Phys. **B524**, 3 (1998).

[10] M.P. Worah, Phys. Rev. Lett. **79**, 3810 (1997); N. Rius and V. Sanz, Nucl. Phys. **B570**, 1555 (2000); J.M. Cline, M. Joyce, and K. Kainulainen, J. High Energy Phys. **07**, 018 (2000).

[11] J.F. Gunion and H.E. Haber, Phys. Rev. D **37**, 2515 (1988); A. Djouadi, Y. Mambrini, and M. Muhlleitner, Eur. Phys. J. C **20**, 563 (2001); J.L. Feng and M.J. Strassler, Phys. Rev. D **55**, 1326 (1997).

[12] D. Atwood, S. Bar-Shalom, G. Eilam, and A. Soni, Phys. Rep. **347**, 1 (2001).

[13] Particle Data Group, K. Hagiwara *et al.*, Phys. Rev. D **66**, 010001 (2002).

[14] R.D. Heuer, D.J. Miller, F. Richard, and P. Zerwas, hep-ph/0106315; ECFA/DESY LC Physics Working Group Collaboration, E. Accomando *et al.*, Phys. Rep. **299**, 1 (1998).

[15] S. Kiyoura, M.M. Nojiri, D.M. Pierce, and Y. Yamada, Phys. Rev. D **58**, 075002 (1998).

[16] G. Passarino and M. Veltman, Nucl. Phys. **B160**, 151 (1979); B.A. Kniehl, Phys. Rep. **240**, 211 (1994).